Resonant tunneling characteristics in crystalline silicon/nanocrystalline silicon heterostructure diodes

Wei Pan, Jia Jia Lu, Jing Chen, and Wen Zhong Shen*
Department of Physics, Laboratory of Condensed Matter Spectroscopy and Opto-Electronic Physics, Shanghai Jiao Tong University, 1954 Hua Shan Road, Shanghai 200030, People's Republic of China
(Received 30 May 2006; revised manuscript received 24 July 2006; published 15 September 2006)

We have carried out a detailed investigation on the resonant tunneling in crystalline (*c*-) Si/nanocrystalline (*nc*-) Si heterostructure diodes, with the emphasis on doping concentration dependence. By the aid of the self-consistent calculation, together with a transfer matrix procedure, we are able to explain well the observed resonant tunneling characteristics under the applied reverse bias in the *c*-Si(*p*)/*nc*-Si(*n*) resonant tunneling diodes. We have demonstrated the controlling of the resonant tunneling by the doping concentrations through modifying the energy levels of the two-dimensional interfacial states and zero-dimensional states in *nc*-Si. The present observation provides us the possibility of realizing unique *nc*-Si device application, such as the easily integrating silicon-based logic gates.

DOI: 10.1103/PhysRevB.74.125308 PACS number(s): 73.40.Gk, 73.63.Kv, 73.40.Lq, 85.35.Be

The resonant tunneling diode (RTD) is one of the most promising devices produced in the field of solid-state nanoelectronics.[1] Many analog/digital multipurpose integrated circuits based on these devices are under developing, such as signal processing, analog-to-digital conversion, communications, and memory.[2] So far, though most of the RTDs are fabricated with mature III-V material, such as GaAs, AlGaAs, InAs, and InP, silicon-based RTDs have received increasing interest due to their easy integration with the mainstream silicon-based circuits.[3] By utilizing nanosilicon-based resonant tunneling devices, unique applications are emerging recently, e.g., the single-electron transistors[4] and the storage nodes in the nanocrystal flash memory.[5,6]

Compared with the artificial silicon quantum dots, the hydrogenated nanocrystalline silicon (*nc*-Si:H), as natural quantum dots embedded in thin (about 2–4 atomic spacings) amorphous Si tissues, has less grain size (3–6 nm), which enables the resonant tunneling a more observable phenomenon.[7,8] We have previously realized the successful growth of *n*-type *nc*-Si:H thin films with high electron mobility on *p*-type crystalline silicon (*c*-Si) substrates by plasma-enhanced chemical vapor deposition (PECVD),[9,10] where unique resonant tunneling phenomena in the *c*-Si(*p*)/*nc*-Si:H(*n*) diodes have been clearly observed.[8] The quantum resonant tunneling effects originate from resonance of the electrons with low-dimensional states, namely, the two-dimensional (2D) states at the *c*-Si/*nc*-Si:H interface and the zero-dimensional (0D) states in the *nc*-Si:H thin film, when an external bias is applied.

Matveev-Larkin (ML) theory[11] has been widely employed to investigate the resonant tunneling between the low-dimensional states. However, it is hard to reveal the underlying device physics by simply using ML theory to illustrate the resonant tunneling characteristics in the *multistate* RTDs,[8] since ML theory focuses on the demonstration of the resonant tunneling processes between *two* given states. As a result, constructing a RTD model based on the quantum transport formalism becomes necessary to gain insight into the mesoscopic transport phenomenon of the *c*-Si/*nc*-Si:H *p-n* RTDs, in which a great number of factors, such as the charge distribution, electron accumulation at the interfaces, and electron-electron interactions, can be taken into account. Furthermore, the comprehensive RTD model can also be used to simulate the structure-dependent quantum transport information to provide guidance for optimal device design, which is indispensable for conceiving unique devices and pursuing realistic device development.

It is well known that the quantum resonant tunneling effects in the *c*-Si/*nc*-Si:H heterostructure *p-n* RTDs can be modified by changing the electronic energy band structure via varying growth parameters in PECVD, such as doping ratio, reactive frequency (rf) power, growth pressure, etc., among which the doping ratio plays the dominant role. In this paper, we have employed the self-consistent calculation, together with the transfer matrix procedure, to explain the observed resonant tunneling in *c*-Si(*p*)/*nc*-Si:H(*n*) heterostructure RTDs. A clear picture of the carrier transport characteristics in these RTDs has been presented. The predicted doping concentration-dependent resonant tunneling characteristics not only have been confirmed by the experiments, but also pave the way for structural controlling of the resonant tunneling in unique *nc*-Si:H device application, such as nanosilicon logic gates.

During the fabrication of *c*-Si(*p*)/*nc*-Si:H(*n*) heterostructure RTD devices, a boron-doped *c*-Si (111) layer ($\sim$10 μm) was first grown by vapor phase epitaxy on a p^+-type Si (100) wafer at 1200 °C. On the top of the *c*-Si thin film, a SiO_2 layer ($\sim$1 μm) was formed by thermal oxidation at 1020 °C, then etched and patterned by photolithography to make an array of square holes (200 μm $\times$ 200 μm), where a fresh phosphorus-doped *nc*-Si:H thin film ($\sim$1 μm) was deposited after appropriate treatments. Finally, Ohmic contacts were made for the *c*-Si(*p*)/*nc*-Si:H(*n*) heterostructure RTDs by evaporating Au-Ti gates and substrate contacts (300 μm $\times$ 300 μm) in vacuum. Figure 1(a) schematically shows the structure of *c*-Si(*p*)/*nc*-Si:H(*n*) heterostructure RTD devices that we use to study the effect of phosphorus doping concentration upon resonant tunneling processes. Figure 1(b) displays the current-voltage (*I-V*) curve measured at 10 K of a

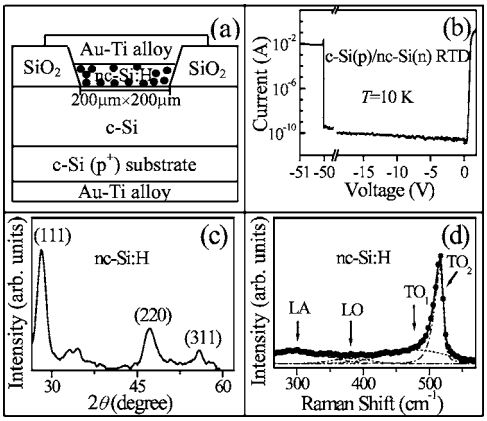

FIG. 1. (a) Cross-sectional view of the *c*-Si(*p*)/*nc*-Si:H(*n*) heterostructure RTDs with geometric parameters. (b) Experimental *I-V* curve for a typical *c*-Si(*p*)/*nc*-Si:H(*n*) heterostructure RTD with a N_{ac} of 1.0×10^{16} cm^{-3} and a N_{dc} of 9.0×10^{15} cm^{-3} measured at 10 K, together with the (c) XRD and (d) Raman spectra of the *nc*-Si:H thin film.

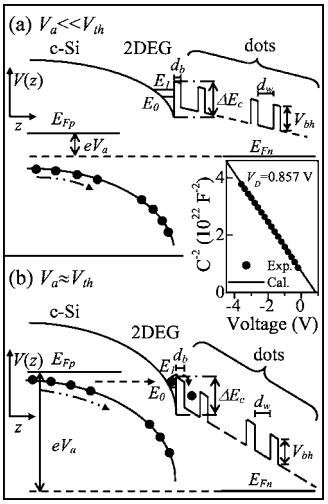

FIG. 2. Schematic energy band diagrams of the *c*-Si(*p*)/*nc*-Si:H(*n*) heterostructure RTDs with the applied reverse bias (a) $V_a \ll V_{th}$ and (b) $V_a \approx V_{th}$. The indicated process is the (a) carrier recombination and (b) tunneling of the electrons via the 2D and/or 0D states. The inset is the capacitance-voltage characteristics measured at 296 K of the typical *c*-Si(*p*)/*nc*-Si:H(n) heterostructure RTD with a N_{ac} of 1.0×10^{16} cm^{-3} and a N_{dc} of 9.0×10^{15} cm^{-3}.

c-Si(*p*)/*nc*-Si:H(*n*) heterostructure RTD with an acceptor concentration N_{ac} of 1.0×10^{16} cm^{-3} and a donor concentration N_{dc} of 9.0×10^{15} cm^{-3}, which exhibits the typical diode characteristics with a rectification ratio of higher than 10^7 at ±0.9 V. It should be noted that we have employed the variable magnetic field Hall measurements, in combination with mobility spectra analysis procedures, to extract the concentrations of the acceptor, donor, and 2D electron gas (2DEG) within the heterostructure RTD samples that are contributing to the transport processes.[9,10]

The phosphorus-doped *nc*-Si:H layers were prepared in a PECVD system by rf (13.56 MHz) and dc bias stimulation. The power density was 0.6 W cm^{-2}, and a negative bias of −200 V was applied to the substrate. A strongly hydrogen diluted silane, i.e., SiH_4 diluted to 1% in H_2, was employed as reactant gas source. Doping was realized by adding PH_3 to the mixed reactant gas, and the doping ratio C_p is defined as PH_3/SiH_4, ranging from 0 to 10 vol. %. Figure 1(c) shows the x-ray diffraction (XRD) spectrum of the same sample as in Fig. 1(b), which was performed at room temperature on a Rigaku Dmax-rc instrument in the standard θ-2θ configuration with a Cu $K\alpha_1$ radiation (1.5406 Å). The good quality of the Si nanocrystals (with an average grain size $d_{(220)}$ of 4.8 nm) is indicated by the relatively sharp and symmetric (111) peak, together with two broad (220) and (311) structures. Raman spectrum of the sample was taken at room temperature using a Jobin Yvon LabRAM HR 800 UV micro-Raman spectrometer with a 514.5 nm line from an Ar^+ laser, and the results [Fig. 1(d)] can be fitted by four Gaussian phonon bands: amorphous longitudinal acoustic (LA) band with a peak at 300 cm^{-1}, amorphous longitudinal optical (LO) band at 380 cm^{-1}, amorphous transverse optical (TO_1) band at 480 cm^{-1}, and crystalline-phase transverse optical (TO_2) band at 524 cm^{-1}. Thus a crystallinity X_C of 54.5% is deduced from $X_C = I_{TO_2}/(I_{TO_2} + \gamma I_{TO_1})$,[12] where I_{TO_1} and I_{TO_2} are integrated intensities of Raman modes centered at 480 and 524 cm^{-1}, respectively. The factor γ is the ratio of the integrated Raman cross section for crystalline silicon to amorphous silicon, which is taken as 0.925 here according to $\gamma = 0.1 + \exp[-d_{(220)}/25]$.[12]

Figure 2 illustrates the schematic energy band diagram of the *c*-Si(*p*)/*nc*-Si:H(*n*) heterostructure RTDs, which can be viewed as the superimposition of the quantum well structure on the heterojunction energy band.[7] The inset of Fig. 2 shows the capacitance-voltage (*C-V*) characteristics measured at 296 K on the *c*-Si(*p*)/*nc*-Si:H(*n*) heterostructure RTD with a N_{ac} of 1.0×10^{16} cm^{-3} and N_{dc} of 9.0×10^{15} cm^{-3}. The linear relationship between C^{-2} and voltage confirms that this RTD is an abrupt graded heterojunction and the intercept of the C^{-2} data with the voltage axis yields a diffusion potential (V_D) of 0.857 V, from which we obtain the conduction-band discontinuity energy (ΔE_c) of *c*-Si(*p*)/*nc*-Si:H(*n*) heterojunctions as ~100 meV. The other energy band quantities about this *c*-Si(*p*)/*nc*-Si:H(*n*) heterostructure RTD shown in Fig. 2 can be obtained from either experiments or literature: the width of the *c*-Si quantum wells (d_w) obtained from the Raman calculation is 4.8 nm, the height of the amorphous Si barriers (V_{bh}) is 60 meV,[13] and the width of the barriers (d_b) between the wells is 1.0 nm.[7] It should be noted that our nanocrystalline in the diodes is uniformly distributed, as demonstrated by the observation of unique resonant tunneling phenomena[8] and high electron mobility.[9,10] The small variation in the grain size (~3% from the simulation of photoluminescence spectra) will result in a slight fluctuation of the 0D-related current peak position and linewidth, which will be negligible when superimposed on the whole strong tunneling current under high reverse bias. As a result, we simply consider an average grain size in the energy band structure for calculation.

Figure 2 also presents the physical pictures of the carrier transport under low and high applied reverse bias V_a. At low reverse biases, as shown in Fig. 2(a), the electrons as the

minority carriers in *c*-Si do not have enough kinetic energy to tunnel into *nc*-Si:H. In this case, the leakage current of the heterostructure plays the dominant role and increases slowly with the applied reverse bias, which has been revealed in Fig. 1(b). When the applied reverse bias reaches a certain value [we denote it as the threshold voltage V_{th}, Fig. 2(b)], the kinetic energy of some electrons in *c*-Si coincides with the energy of the 2D states in the interface and/or 0D states in *nc*-Si:H, and will resonate with these low-dimensional states, leading to the appearance of the tunneling current peak in Fig. 1(b). Therefore, though the tunneling effect looks like that of Esaki diodes in semiconductor *p-n* junctions, this kind of tunneling to the low-dimensional states in the special 3D-2D-0D system is a typical resonant tunneling phenomenon, instead of the band to band tunneling Esaki diodes based on density of states effects.

The tunneling current in quantum wells, superlattices and double-barrier tunneling diodes has been widely investigated. The reported tunneling current in the above structures can be obtained by calculating the transmission coefficient using the transfer matrix procedure,[14] followed by the current density calculation with the aid of the Tsu-Esaki formula.[15] We shall adopt a similar method to simulate the tunneling current characteristics in the *c*-Si(*p*)/*nc*-Si:H(*n*) heterostructure RTDs, in which the unknown vertical effective potential energy distribution in the space charge region is obtained by the self-consistent calculation. We start with the potential energy $V(z)$ in the space charge region of the heterojunction, which can be expressed as

$$V(z) = -e\phi(z) + V_h(z) + V_{xc}(z), \tag{1}$$

where $\phi(z)$ is the electrostatic potential, $V_h(z)$ is the effective potential energy associated with the (graded) heterojunction discontinuity, and $V_{xc}(z)$ is the local exchange-correlation potential energy. Although we have demonstrated in the *C-V* measurements that the studied RTD is an abrupt graded heterojunction, a mathematical abrupt transition cannot be realized in the real heterojunction structure. In order to treat theoretically the out-of-flatness at the interface, we have defined $V_h(z)$ as a graded function with a 0.5 nm transition layer, which represents the potential transition process from *c*-Si to *nc*-Si:H. The detailed description of the calculation procedures on $V_h(z)$ and $V_{xc}(z)$ can be found elsewhere.[16]

The normalized envelope function $\xi_i(z)$ for an electron in subband *i* is assumed to be given by a Schrödinger equation of the BenDaniel-Duke form[17]

$$-\frac{\hbar^2}{2}\frac{d}{dz}\frac{1}{m(z)}\frac{d\xi_i(z)}{dz} + V(z)\xi_i(z) = E_i\xi_i(z), \tag{2}$$

where $m(z)$ is the position-dependent effective mass and E_i is the energy of the bottom for the *i*th subband. Furthermore, Poisson equation for the electrostatic potential (in SI units) takes the form

$$\frac{d}{dz}\varepsilon_0\kappa(z)\frac{d\phi(z)}{dz} = e\sum N_i\xi_i^2(z) - \rho_I(z), \tag{3}$$

$$N_i = \frac{m_c k_B T}{\pi\hbar^2}\ln\left[1 + \exp\left(\frac{E_F - E_i}{k_B T}\right)\right], \tag{4}$$

where $\kappa(z)$ is the position-dependent dielectric constant, N_i is the number of electrons per unit area in the *i*th subband, E_F is the Fermi energy, and m_c is the effective mass in *c*-Si, where subscript *c* is used to denote the *c*-Si (channel) side of the heterojunction.

The impurity charge density $\rho_I(z)$ used in Eq. (3) can be expressed as a piecewise function for an abrupt graded heterojunction

$$\rho_I(z) = \begin{cases} -eN_{ac} & (z < 0) \\ eN_{dc} & (z > 0), \end{cases} \tag{5}$$

with N_{ac} the acceptor concentration in *c*-Si, and N_{dc} the donor concentration in *nc*-Si:H. It should be noted that the potential energy at the interface is referenced as the zero energy point. Given the impurity charge density profile, the effective potential energy $V(z)$ in the space charge region can therefore be calculated by self-consistently solving the Schrödinger and Poisson equations. The four-ordered Runge-Kutte method[18] has been used to solve both the Schrödinger and Poisson equations. The triangle potential energy is served as the initial input potential energy, and the iteration is interrupted when the difference between the output and the input potential energy is smaller than 10^{-6} eV. The validity of the program has been examined for the GaAs/AlGaAs heterojunction in Ref. 16.

Finally, the tunneling current *J* at different reverse biases is obtained via the formula[19]

$$J \propto \int T(E)\frac{\partial F}{\partial E}dE, \tag{6}$$

where $T(E)$ is the transmission coefficient, *E* is the energy of the incident electron, and *F* is the distribution function. Here we have employed the standard transfer matrix procedure[14] to evaluate the transmission coefficient $T(E)$ of the electrons through the vertical potential energy, which has been obtained by the superimposition of the quantum well structure and the effective potential energy $V(z)$ in Eq. (1). As for the electron distribution function *F*, it is assumed that under a certain applied reverse bias V_a, *F* follows the normal distribution function which centers at $E_b = \alpha e V_a$,[20] with α the ratio of the obtained energy of the electrons to the electrostatic potential across the heterojunction, which is defined as the energy gaining ratio of the electrons in *c*-Si.

We have noticed that much work has been done on highly-accurate, multiband calculations for RTDs,[21–26] especially for hole and interband tunneling devices to incorporate the realistic valence band structure and the mixing of the conduction band state with the valence band heavy- and light-hole states. The numerical instability problem has been solved well[21,22] in the transfer matrix method used in conjunction with the multiband models. The importance of in-plane wave vector in the transmission coefficient has also been recognized by Kiledjian *et al.*[23] and Boykin *et al.*[24] Furthermore, Bowen *et al.*[25] have discussed the effect of Hartree self-consistent potentials on the band structure pro-

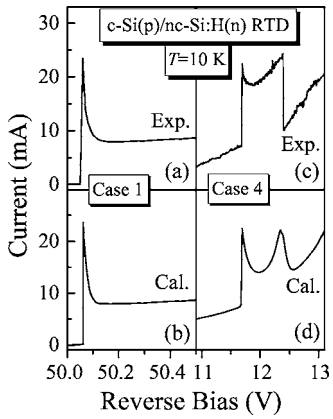

FIG. 3. (a) Experimental and (b) calculated tunneling current characteristics of the *c*-Si(*p*)/*nc*-Si:H(*n*) heterostructure RTD with a N_{ac} of 1.0×10^{16} cm^{-3} and a N_{dc} of 9.0×10^{15} cm^{-3} at 10 K. (c) Experimental and (d) calculated tunneling current characteristics of another *c*-Si(*p*)/*nc*-Si:H(*n*) heterostructure RTD with a N_{ac} of 7.6×10^{14} cm^{-3} and a N_{dc} of 1.0×10^{17} cm^{-3} at 10 K.

files and resonant tunneling in RTDs working at high temperatures, e.g., room temperature, where we have to employ the nonequilibrium Green's function technique to accurately model the quantum electron transport characteristics.[26] Nevertheless, in our present *c*-Si(*p*)/*nc*-Si:H(*n*) RTDs with normal electron tunneling, the theoretical treatment can be simplified into the above envelope-function theory without the instability problem and in-plane wave vector dependence. As will be demonstrated below, this simple envelope-function theory can predict well the doping concentration-dependent tunneling current characteristics at very low temperature of 10 K.

Figure 3(a) displays an isolated current peak observed in the *I-V* curve measured at 10 K for the *c*-Si(*p*)/*nc*-Si:H(*n*) heterostructure RTD with a N_{ac} of 1.0×10^{16} cm^{-3} and a N_{dc} of 9.0×10^{15} cm^{-3}. It is clear that the reverse current exhibits a step jump at the threshold voltage of ~50 V, followed by an exponential decay, which indicates the existence of the electron-electron interactions.[27] Figure 3(b) gives the calculated *I-V* curve as a sum of the tunneling current based on our above model and the leakage current of the RTD with the aforementioned energy band parameters. One can observe that the theoretical current characteristics agree quite well with the experimental data.

The calculation indicates that the observed isolated current peak in the I-V curve originates from the three-dimensional state (3D) in *c*-Si to the interfacial 2D state tunneling, because it is found that when the resonant tunneling occurs, the kinetic energy of the incident electrons is identical to the energy E_0 (34.13 meV) of the first subband in the 2D states (see Fig. 2). The 0D states energy (E_{0D}) in *nc*-Si:H, which is near E_0 but about 6 meV lower than E_0, does not contribute to the resonant tunneling in this scenario. Furthermore, due to the very small energy gaining ratio α of 0.008, the energy that the electrons get at the threshold voltage is 400 meV higher than that at zero bias, requiring a large threshold bias ($V_{th}\approx50$ V) for observing the 3D-2D tunneling. The calculation also reveals an exponential decay of the current following the tunneling peak, and then a gradually increasing tendency towards the breakdown region of the heterostructure.

Therefore, the whole transport process related to this *I-V* structure can be clarified as follows: When the applied reverse bias is up to the threshold voltage, the electrons in *c*-Si will obtain enough energy to be resonant with the 2D states and tunnel into the *nc*-Si:H thin film, leading to the tunneling current instead of the leakage current that plays the dominant role in the common situation. With the further increase of the reverse bias, the resonant tunneling condition is destroyed, and due to the existence of the electron-electron interactions, the current exhibits an exponential decay. However, since the threshold voltage is near the breakdown region of the heterostructure, the breakdown phenomenon immediately enforces the current to show the observed gradual increase.

It should be noted that only when the applied reverse bias reaches the threshold voltage V_{th} and the electrons in *c*-Si resonate with first the 2D states can the resonant tunneling be observed. This explains the reason why we could not observe the contribution of 0D states in the above resonant tunneling is that E_{0D} is about 6 meV lower than E_0 under the threshold voltage in the studied *c*-Si(*p*)/*nc*-Si:H(*n*) RTD. However, this argument provides us the base to investigate into the resonant tunneling characteristics, including the contribution of the 0D states, in relationship with the energy levels of the 2D and 0D states, which can be directly modified by the doping concentrations through controlling the electronic energy band via the effective potential distribution. We have chosen four typical cases of *c*-Si(*p*)/*nc*-Si:H(*n*) heterostructure RTDs, as listed in Table I, to demonstrate the effect of the doping concentrations on the resonant tunneling.

Figure 4(a) displays the calculated conduction-band dia-

TABLE I. Acceptor concentration N_{ac} in *c*-Si and donor concentration N_{dc} in *nc*-Si:H used in the theoretical simulations of resonant tunneling in *c*-Si(*p*)/*nc*-Si:H(n) heterostructure RTDs, and the calculated 2D state energy E_0 at the applied reverse bias V_a reaching the threshold voltage V_{th}, together with the resonant energy E_{res} and the energy gaining ratio α.

Cases	N_{ac} (cm^{-3})	N_{dc} (cm^{-3})	$E_0(V_a=V_{th})$ (meV)	V_{th} (V)	E_{res} (meV)	$\alpha=E_{res}/V_{th}$
1	1.0×10^{16}	9.0×10^{15}	34.13	50.06	400.84	0.008
2	7.6×10^{14}	5.0×10^{16}	20.26	15.20	120.51	0.008
3	7.6×10^{14}	8.0×10^{16}	20.26	12.04	96.32	0.008
4	7.6×10^{14}	1.0×10^{17}	20.26	11.69	82.17	0.007

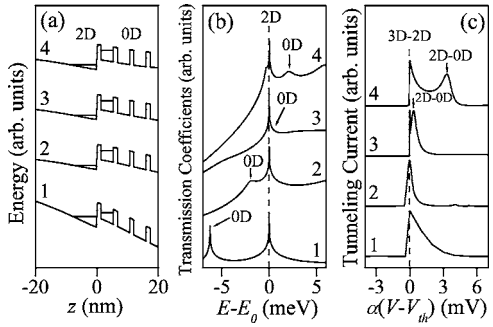

FIG. 4. Calculated (a) conduction-band energy diagrams at zero bias, (b) corresponding transmission coefficient spectra at the threshold voltage, and (c) tunneling current spectra of the *c*-Si(p)/*nc*-Si:H(n) heterostructure RTDs with four typical cases of doping concentrations: 1. $N_{ac}=1.0\times10^{16}$ cm^{-3} and $N_{dc}=9.0\times10^{15}$ cm^{-3}; 2. $N_{ac}=7.6\times10^{14}$ cm^{-3} and $N_{dc}=5.0\times10^{16}$ cm^{-3}; 3. $N_{ac}=7.6\times10^{14}$ cm^{-3} and $N_{dc}=8.0\times10^{16}$ cm^{-3}; and 4. $N_{ac}=7.6\times10^{14}$ cm^{-3} and $N_{dc}=1.0\times10^{17}$ cm^{-3}.

grams of the RTDs with those sets of different concentrations at zero bias, which clearly exhibits the modification of electronic energy band in the space charge region and the energy levels of the 2D and 0D states. The slope of the energy band decreases with the decreasing N_{ac} in the *c*-Si side, and decreases with the increasing N_{dc} in the *nc*-Si:H side, leading to the lowering of the energy position of the 2D states and elevation of the 0D states. With the increase of the applied reverse bias, the position of E_0 rises while E_{0D} drops. Figure 4(b) gives the corresponding transmission coefficient spectra, normalized to the lowest subband E_0 of the 2D states, under the applied reverse bias of $V_a=V_{th}$. Table I also lists the values of E_0, which are mainly determined by N_{ac}. In addition to the main 2D peak, another structure related to the 0D states can be clearly observed. It is found that with the decrease of N_{ac} in *c*-Si and increase of N_{dc} in *nc*-Si:H, the position of the 0D states (E_{0D}) relative to E_0 is lifted, where the 0D peak overlaps with the main 2D one in the case 3, and lies above it in the case 4.

The variation of the 0D peak in transmission coefficient spectra will no doubt influence the tunneling current in *c*-Si(p)/*nc*-Si:H(n) heterostructure RTDs. Figure 4(c) shows the calculated resonant tunneling current of the four typical RTDs normalized to the threshold voltage V_{th} for a better visualization. The values of V_{th}, listed in Table I, were obtained through dividing the calculated resonant energy E_{res} by the energy gaining ratio α. It is found that V_{th} decreases with N_{ac} and/or the increasing N_{dc}, as a result of the Fermi energy level in *c*-Si approaching to E_0, where less energy is needed for the electrons to resonate with the 2D states. As we know, the position of E_0 rises while E_{0D} drops with the increase of the applied reverse bias. If E_0 is lower than E_{0D} when the electrons in *c*-Si resonate with the 2D states, further increase of the reverse bias will cause the position of E_0 to be aligned with that of E_{0D}, leading to the appearance of 2D-0D resonant tunneling. On the other hand, if E_0 is higher than E_{0D} when the reverse bias reaches the threshold voltage, there is no chance for the coincidence of E_0 and E_{0D} with the increase of the applied bias, i.e., only single 3D-2D tunneling peak, as in the case of Fig. 3(a), can be observed. The calculated resonant tunneling results of Fig. 4(c) clearly demonstrate the above argument by revealing the evolution of the 2D-0D peak with the relative position of the 0D transmission coefficient peak to the 2D one in Fig. 4(b). It is clear that the separation between the 3D-2D and 2D-0D tunneling peaks can also be tuned easily by the doping concentrations.

We have further fabricated the case 4 *c*-Si(p)/*nc*-Si(n) RTD with a $N_{ac}\sim7.6\times10^{14}$ cm^{-3} and a $N_{dc}\sim1.0\times10^{17}$ cm^{-3} to confirm the theoretical expectations. Figure 3(c) displays the experimental reverse *I*-*V* curve measured at 10 K, where two resonant tunneling current peaks (3D-2D and 2D-0D) can be clearly observed. Figure 3(d) shows the calculated current, which includes both the tunneling current and the leakage current, revealing good agreement with the experimental observation. Furthermore, from the calculated resonant energy E_{res} of this RTD and the experimental threshold voltage of 11.69 V, we have yielded a value of 0.007 for the energy gaining ratio α in this sample, close to the result of 0.008 in the case 1 RTD, indicating that α is almost independent of the energy band diagrams of the RTDs. In addition, it is worth noting that we have already reported in Ref. 8 the 0D-0D resonant tunneling with the further increase of the applied reverse bias, therefore all the resonant tunneling processes related to the 2D and 0D states have been revealed in the *c*-Si(p)/*nc*-Si:H(n) RTDs.

Finally, we would like to emphasize that the above controlling of the resonant tunneling characteristics via the doping concentrations through modifying the energy levels of the 2D and 0D states provides us the possibility of satisfying the different demands on the *nc*-Si:H based device design. For example, for the digital circuit devices, such as the logic gates, it is usual to utilize the bistable characteristics in the resonant tunneling, and then increase the separation between the two peaks to increase the output noise margin.[28] Our present observation indicates that, by the aid of doping concentration controlling, we cannot only demonstrate the transition of the resonant tunneling characteristics from the monostable state (single-peak structure) to bistable state (double-peak structure) in the *c*-Si/*nc*-Si:H *p*-*n* RTDs, but also modulate the threshold voltage as well as the separation between these two tunneling peaks. In other words, by choosing appropriate doping concentrations, we can realize the *nc*-Si:H based logic gates, easy integration with the current silicon circuits, where the operating voltage and output noise margin can be easily optimized via reducing the threshold voltage and increasing the separation of the tunneling peaks.

In summary, we have presented a clear picture of the carrier transport in *c*-Si(p)/*nc*-Si:H(n) heterostructure RTDs and demonstrated the controlling of the resonant tunneling via the doping concentrations through modifying the energy levels of the 2D interfacial states and 0D states in *nc*-Si:H. It is found that the resonant tunneling current will transfer from single-peak to double-peak structures with the threshold voltage and separation between the two peaks easily being tuned. The present observation provides us the possibility of realizing unique *nc*-Si:H logic gates, which are easy integration with the mainstream silicon-based technology. While the

simple envelope-function theory can explain successfully the resonant tunneling phenomena in our *c*-Si(*p*)/*nc*-Si:H(*n*) RTDs under the applied reverse bias, more accurate multiband models will be needed to describe the hole tunneling in *c*-Si(*n*)/*nc*-Si:H(*p*) RTDs and temperature-dependent tunneling current characteristics of these nanosilicon-based devices.

This work is supported by the Natural Science Foundation of China under Contracts No. 10125416 and No. 60576067, and Shanghai Municipal Commission of Science and Technology Projects of 05DJ14003, 05QMH1411, and 06JC14039, as well as the National Minister of Education Program for Changjiang Scholars and Innovative Research Team in University (PCSIRT).

*Corresponding author. Email address: wzshen@sjtu.edu.cn

[1] I. I. Abramov, I. A. Goncharenko, and N. V. Kolomeîtseva, Semiconductors **39**, 1102 (2005).
[2] P. Mazumder, S. Kulkarni, M. Bhattacharya, J. P. Sun, and G. I. Haddad, Proc. IEEE **86**, 664 (1998).
[3] L. Geppert, IEEE Spectrum **37**, 46 (2000).
[4] Y. Inoue, A. Tanaka, M. Fujii, S. Hayashi, and K. Yamamoto, J. Appl. Phys. **86**, 3199 (1999).
[5] S. Tiwari, F. Rana, H. Hanafi, A. Hartstein, E. F. Crabbé, and K. Chan, Appl. Phys. Lett. **68**, 1377 (1996).
[6] S. Huang, S. Banerjee, R. T. Tung, and S. Oda, J. Appl. Phys. **93**, 576 (2003).
[7] Y. L. He, G. Y. Hu, M. B. Yu, M. Liu, J. L. Wang, and G. Y. Xu, Phys. Rev. B **59**, 15352 (1999).
[8] X. Y. Chen and W. Z. Shen, Appl. Phys. Lett. **85**, 287 (2004).
[9] X. Y. Chen and W. Z. Shen, Phys. Rev. B **72**, 035309 (2005).
[10] X. Y. Chen, W. Z. Shen, and Y. L. He, J. Appl. Phys. **97**, 024305 (2005).
[11] K. A. Matveev and A. I. Larkin, Phys. Rev. B **46**, 15337 (1992).
[12] B. Garrido, A. Pérez-Rodríguez, J. R. Morante, A. Achiq, F. Gourbilleau, R. Madelon, and R. Rizk, J. Vac. Sci. Technol. B **16**, 1851 (1998).
[13] S. Gall, R. Hirschauer, M. Kolter, and D. Bräunig, Sol. Energy Mater. Sol. Cells **49**, 157 (1997).
[14] Y. Ando and T. Itoh, J. Appl. Phys. **61**, 1497 (1986).
[15] R. Tsu and L. Esaki, Appl. Phys. Lett. **22**, 562 (1973).
[16] F. Stern and S. Das Sarma, Phys. Rev. B **30**, 840 (1984); S. V. Kravchenko, J. M. Caulfield, J. Singleton, H. Nielsen, and V. M. Pudalov, *ibid.* **47**, 12961 (1993).
[17] D. J. BenDaniel and C. B. Duke, Phys. Rev. **152**, 683 (1966).
[18] W. H. Press, S. A. Teukolsky, W. T. Vetterling, and B. P. Flannery, *Numerical Recipes in C: The Art of Scientific Computing*, 2nd ed. (Cambridge University Press, Cambridge, 1992).
[19] D. Embriaco and G. C. La Rocca, Solid State Commun. **117**, 407 (2001).
[20] A. Kojima and N. Koshida, Phys. Status Solidi A **197**, 452 (2003).
[21] T. B. Boykin, J. P. A. van der Wagt, and J. S. Harris, Jr., Phys. Rev. B **43**, 4777 (1991).
[22] D. Z. Y. Ting, E. T. Yu, and T. C. McGill, Phys. Rev. B **45**, 3583 (1992).
[23] M. S. Kiledjian, J. N. Schulman, K. L. Wang, and K. V. Rousseau, Surf. Sci. **267**, 405 (1992); Phys. Rev. B **46**, 16012 (1992).
[24] T. B. Boykin, R. E. Carnahan, and K. P. Martin, Phys. Rev. B **51**, 2273 (1995); T. B. Boykin, *ibid.* **51**, 4289 (1995).
[25] R. C. Bowen, G. Klimeck, R. K. Lake, W. R. Frensley, and T. Moise, J. Appl. Phys. **81**, 3207 (1997).
[26] R. Lake, G. Klimeck, R. C. Bowen, and D. Jovanovic, J. Appl. Phys. **81**, 7845 (1997).
[27] A. K. Geim, P. C. Main, N. La Scala Jr., L. Eaves, T. J. Foster, P. H. Beton, J. W. Sakai, F. W. Sheard, M. Henini, G. Hill, and M. A. Pate, Phys. Rev. Lett. **72**, 2061 (1994).
[28] D. P. Nackashi, C. J. Amsinck, N. H. DiSpigna, and P. D. Franzon, Proceedings of the 5th IEEE Conference on Nanotechnology, 2005, Vol. 2, p. 819.